

Modulating Tumor Extracellular Matrix by Simultaneous Inhibition of Two Cancer Cell Receptors

Weizhi Chen, Yang Yuan, Cheng Li, Hui Mao, Baorui Liu, and Xiqun Jiang*

The extracellular matrix (ECM) is involved in fundamental cellular processes and pathological progression of many diseases. While most research and current knowledge focuses on the processes of biological and mechanical changes in ECM signaling residing cancer cells to respond, little is known of the converse—of how cancer cells initiate the changes of ECM properties. Here, it is reported that blocking the cancer cell signaling leads to disruption of tumor ECM. Using recombinant proteins (RPs) and recombinant protein-drug conjugates (RPDCs) that simultaneously target both epidermal growth factor receptor and integrin, it is demonstrated that multireceptor-mediated active modulation of tumor ECM can inhibit and even reverse tumor remodeling of the physiological and structural microenvironment. These results not only provide insights into the regulatory roles of cancer cells in developing a protumoral microenvironment, but also introduce a new therapeutic platform or strategy to treat cancers.

1. Introduction

Extracellular matrix (ECM) plays key roles in fundamental cellular processes and pathological progression of many diseases, including cancer, fibrosis, and cardiovascular disease.^[1–3] For example, ECM is a main component of the tumor microenvironment (TME) in cancer development and progression.^[4] The stiffness of ECM strongly affects both physiological and mechanical properties of the tumor tissue, therefore profoundly influencing tumor invasion, metastasis, drug resistance, and angiogenesis.^[5–7] A stiff ECM promotes cancer cell growth and metastasis, while also perpetuating resistance to therapies.^[8–12] In contrast, a soft ECM suppresses angiogenesis and DNA repair, and increases tumor sensitivity to chemotherapy and radiotherapy.^[13] Thus, targeting ECM to disrupt TME is a logical

approach to develop new cancer therapies. However, controlling or reversing the tumor ECM and its stiffness in an activatable manner to enhance tumor responses to the therapy remains challenging and requires better understanding of cell–matrix interactions, particularly, how cancer cells initiate or signal the tumorigenic changes in ECM and eventually the protective TME.

While most existing studies focus on the mechanisms involving biological and mechanical changes in ECM that signal cancer cells to respond,^[14,15] little is known on how cancer cells cause changes in ECM properties. In contrast to studies that investigated the effects of ECM on cellular behaviors in vitro using various model systems,^[6,10,16,17] replicating the biological and mechanical changes of ECM in vivo

is much more difficult due to limited information about which cell signaling molecules are associated with the initiation of changes in ECM composition and stiffness. A further challenge is the dynamic and transient nature of changes in ECM properties in response to cell signals, which cannot be recapitulated in vitro using models.

Here, we propose and demonstrate a strategy of using multireceptor mediated active modulation of tumor extracellular matrix (mRMM–ECM) to block cancer cell signaling to softened tumor ECM and disrupted TME. These antitumoral changes in ECM composition and stiffness can be achieved by simultaneously blocking two key receptors—epidermal growth factor receptor (EGFR) and integrin, which are overexpressed in cancer cells.

Integrins, cell surface adhesion receptors known to be overexpressed in most cancer cells,^[18] play key roles in cancer cells migration and invasion and tumor stiffness.^[19,20] Moreover, the overexpression of integrins facilitates interactions between tumor cells and collagens in ECM,^[21] leading to the activation of the fibroblast in ECM, which further stimulates the collagen generation.^[22] This dense collagen network and the activated fibroblasts production make the tumor more fibrotic and stiff.^[9]

Integrins also connect ECMs with cell cytoskeleton by linking their extracellular domains with ECM and intracellular domains with actin cytoskeleton to regulate cell tension.^[23] On the other hand, overexpression of EGFR, one of the hallmark events in cancers,^[24] upregulates the integrin tension coupled with reorganization of focal adhesions.^[25] The interplay of EGFR and integrin and its subsequent alterations in ECM promote tumors to develop a stiff TME that hinders the

W. Chen, Y. Yuan, C. Li, X. Jiang
College of Chemistry and Chemical Engineering
Nanjing University
Nanjing 210023, China
E-mail: jiangx@nju.edu.cn

H. Mao
Department of Radiology and Imaging Sciences
Emory University
Atlanta, GA 30322, USA

B. Liu
The Comprehensive Cancer Centre of Drum Tower Hospital
Medical School of Nanjing University
Nanjing 210008, China

 The ORCID identification number(s) for the author(s) of this article can be found under <https://doi.org/10.1002/adma.202109376>.

DOI: 10.1002/adma.202109376

delivery of exogenous therapeutic agents, such as small drugs, antibodies, and immune cells, to the tumor.^[26,27] Thus, simultaneously inhibiting EGFR and integrin expression in ECM-residing cancer cells could generate a synergistic disruption of the cancer cell signaling that stiffens ECM. To do this, we used EGFR and integrin dual-targeted recombinant proteins (RP-ER) and recombinant protein-drug conjugates (RPDC-ER) and demonstrated that the RPDCs can stop, or even reverse, tumor remodeling of the physiological and structural microenvironment. Consequently, the RPDCs capable of mRMM-ECM can improve the delivery and intratumor distribution of potential therapeutics in a softened tumor mass, leading to a significantly improved antitumor efficacy.

2. Results

2.1. Design of RP-ER and RPDC-ER

Using a combination of EGFR-specific inhibitors and tumor integrin inhibitors is a common approach in improving the specificity and efficacy of cancer treatment.^[28–30] However, the conventional coadministration of both inhibitors lacks precise

control of their stoichiometry and distribution to achieve the desired synergistic effect. To achieve highly localized, stoichiometric, and simultaneous inhibitions of both targets, we designed a dual-targeting RPDC consisting of four key functional components: the EGFR-specific anti-EGFR nanobody,^[31] integrin $\alpha_v\beta_3$ -bound cyclic peptide,^[32] C-RGD-KGPDC (RGD), the elastin-like polypeptide with multifunctional groups,^[33] and an acid-labile hydrazone moiety to link the selected drug molecules. In contrast with a conventional antibody, the nanobody used in this study has several advantages including small size, great penetration ability, and easily constructable bispecific RPs.^[34,35] Four types of recombinant proteins (RPs)—prime elastin-like polypeptide (RP), RGD-chimeric RP (RP-R), anti-EGFR nanobody-chimeric RP (RP-E), chimeric RP with both RGD, and anti-EGFR nanobody (RP-ER)—were expressed from *Escherichia coli* (*E. coli*) (Figure 1A; and Figure S1A, Supporting Information). Only RP-ER consists of two targeting moieties, i.e., anti-EGFR nanobody and integrin ligand. RP without target ligand, integrin-targeted RP-R, and EGFR-targeted RP-E were used as control samples. The purities and molecular weights of the four RPs were first measured by sodium dodecyl sulfate polyacrylamide gel electrophoresis (Figure S1B, Supporting Information). Matrix-assisted laser desorption/ionization

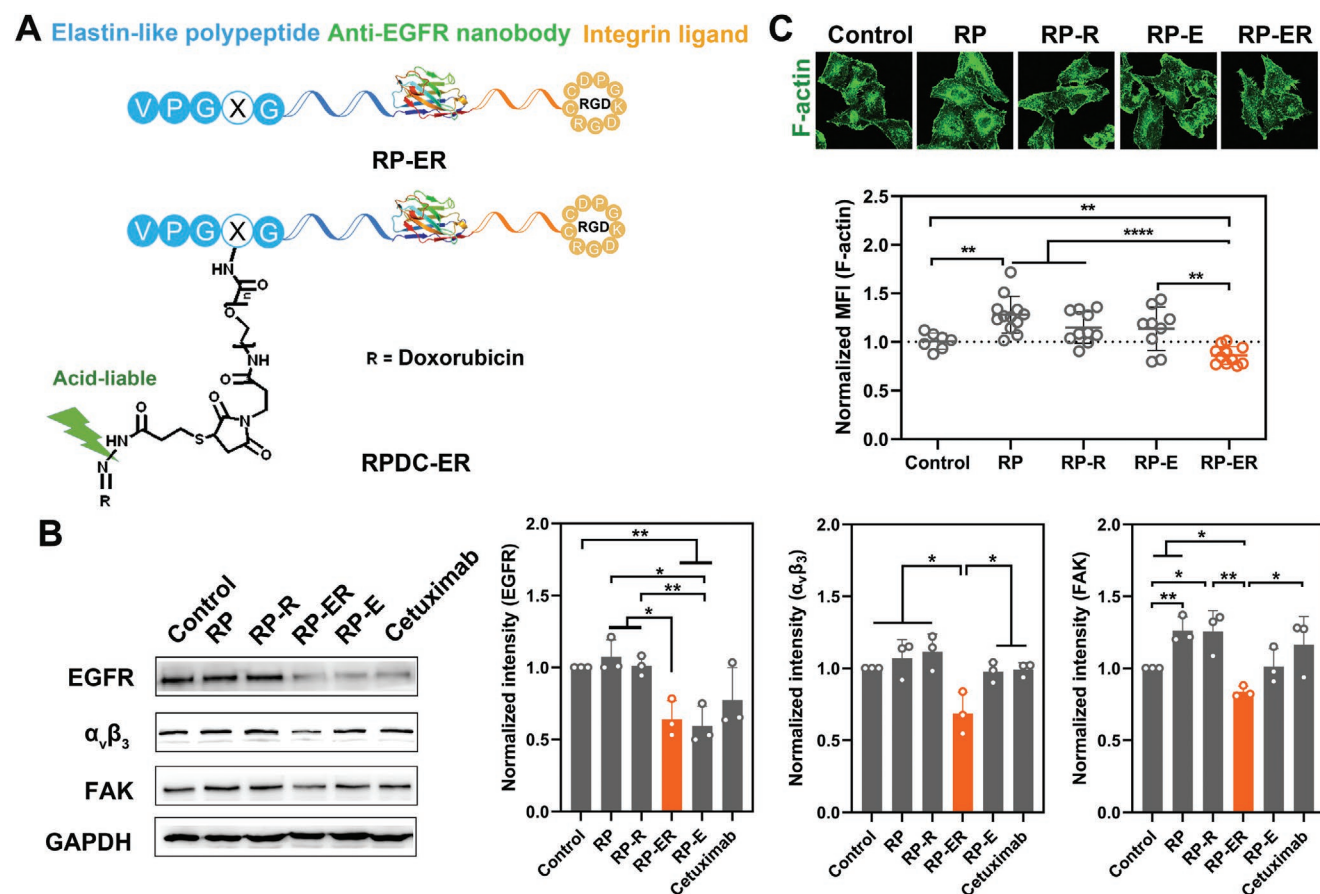


Figure 1. RP-ER reduces the expression of specific biomarkers in HeLa cells. A) RP-ER consisting of a nanobody against EGFR and a RGD peptide that binds integrin was expressed from *E. coli*, followed by chemical conjugation with DOX through the pH-sensitive hydrazone bond and a polyethylene glycol oligomer spacer to form RPDC-ER. B) RP-ER downregulates the expressions of EGFR, integrin $\alpha_v\beta_3$, and FAK in HeLa cells. Intensities in western blots were normalized by ImageJ ($n = 3$). C) RP-ER reduces F-actin content in HeLa cells. The MFIs were normalized ($n = 7–11$). Data are presented in mean \pm sd. *P* values were calculated using multiple *t*-tests. * $P < 0.05$, ** $P < 0.01$, **** $P < 0.0001$.

time-of-flight mass spectrometry was then used to determine the molecule weights of RP, RP-R, RP-E, and RP-ER, which were 21 kDa (Figure S1C, Supporting Information), 23 kDa (Figure S1D, Supporting Information), 38 kDa (Figure S1E, Supporting Information) and 40 kDa (Figure S1F, Supporting Information), respectively. The molecular structures of the four RPs were confirmed by circular dichroism spectra (Figure S1G, Supporting Information). A strong positive band at ≈ 198 nm and a strong negative band at ≈ 218 nm were observed, suggesting that RP-ER is composed of both β -sheet secondary conformation from anti-EGFR nanobody and disordered structure from elastin-like polypeptide.^[36,37]

An antitumor agent, doxorubicin (DOX), was covalently linked to RPs through the pH-sensitive hydrazone bond and a polyethylene glycol oligomer spacer to form the four different RPDCs, i.e., RPDC, RPDC-R, RPDC-E, and RPDC-ER, respectively (Figure 1A). The UV-vis absorption spectra of RPDCs exhibited the same profiles as free DOX (Figure S2A, Supporting Information). The zeta potentials of the RPDCs were reduced after drug conjugation due to the neutralization of the amine groups in the lysine residues of RPs (Figure S2B, Supporting Information), suggesting that DOX was successfully conjugated with the RPs and the designed RPDCs were obtained. The hydrodynamic radius of the four RPDCs were 3.8, 3.9, 5.0, and 5.1 nm (Figure S2C, Supporting Information), respectively. Each RPDC carried an average of two DOX molecules (Figure S2D, Supporting Information) with a pH-responsive drug release behavior (Figure S2E, Supporting Information) suitable for the controlled release of drugs in the weak acidic tumor tissues (Figure S2F, Supporting Information).^[38,39] All RPDCs showed a concentration-dependent cytotoxicity in HeLa cells (Figure S2G, Supporting Information), with RPDC-ER exhibiting the lowest IC₅₀ value among the four RPDCs (Figure S2D, Supporting Information). Cytocompatibility of the four RPs was also evaluated using NIH3T3 cells (Figure S2H, Supporting Information). No cytotoxicity for normal NIH3T3 cells was found for all the RPs even at the highest concentration ($400 \mu\text{g mL}^{-1}$). Because RP-ER can target both EGFR and integrin, RP-ER exhibited a higher level of cellular internalization than single-receptor targeting RPDCs in a receptor-mediated pathway (Figure S3A,B, Supporting Information). The cell internalization of RP-ER by EGFR-positive HeLa cells were 5.9, 3.9, and 1.3 folds higher than RP, RP-R, and RP-E, respectively. When the cells were pretreated with EGFR-specific monoclonal antibody cetuximab, the cell uptake of RP-ER was significantly decreased (Figure S3B, Supporting Information).

2.2. RP-ER Reduces the Expressions of Specific Biomarkers and Enhance Cellular Uptake

To determine the effect of different RP on the expressions of EGFR, integrin, and focal adhesion kinase (FAK), western blotting analysis were performed in EGFR-positive HeLa cells using phosphate buffer saline (PBS) and cetuximab as controls (Figure 1B). Only the RP-ER with simultaneous dual-targeting of EGFR and integrin had significant effects on the intracellular downregulations of both EGFR and $\alpha_v\beta_3$ compared to the agents that singularly target either EGFR or integrin. A

40% reduction of both EGFR and $\alpha_v\beta_3$ levels in the cells was observed for RP-ER.

We also observed the decreased level of FAK, which senses mechanical and biological cues from the environment to the cells.^[40] Stimulation of the cells with the epidermal growth factor (EGF) yielded similar results (Figure S3C, Supporting Information)—that is, only the EGFR and integrin dual-targeting RP-ER was capable of significantly lowering the expression levels of EGFR, integrin, and FAK in cancer cells simultaneously with EGF stimulation. Simultaneous downregulation of the expressions of EGFR, $\alpha_v\beta_3$, and FAK by RP-ER was also found in different cancer cell lines, including breast cancer MCF-7 (Figure S4A, Supporting Information) and MDA-MB 231 cells (Figure S4B, Supporting Information), lung cancer A549 cells (Figure S4C, Supporting Information), and pancreatic cancer MIA PaCa-2 cells (Figure S4D, Supporting Information), suggesting that the inhibiting effect on cancer cell signaling by dual-targeting is not cell type specific. The downregulating effect of RP-ER on these biomarkers of the cancer cells was also evaluated at the mRNA level. Lower mRNA levels of *EGFR*, *ITGAV*, *ITGB3*, and *PTK2* (codes for FAK) with RP-ER treatment was also found in the tested cancer cells (Figure S4E-I, Supporting Information).

When evaluating the level of intracellular F-actin (a cytoskeletal protein that controls cell tension and various cell uptake and efflux processes^[41]) using FITC-labeled phalloidine, we found that RP-ER decreased the F-actin content by 16% (Figure 1C). As a result of RP-ER treatment, the free rhodamine B (RB) uptake by HeLa cells was significantly enhanced. A 1.6-fold increase in cell internalization of RB was observed when the cells were coincubated with RP-ER and free RB (Figure 2A,B). This was similar to increasing or decreasing the cellular uptake of RB by a 10 min pretreatment of 300×10^{-9} M cytochalasin D (CyD) or 50×10^{-6} M arachidonic acid (AA) (Figure 2C–E) to modulate microfilament contents of F-actin.^[42,43] Pretreatment with CyD led to truncation of F-actin, resulting in higher RB uptake in HeLa cells. In contrast, AA treatment accelerated actin polymerization and reduced the cell internalization ability. Decreased F-actin content with RP-ER treatment was also found in MCF-7 cells (Figure S5A, Supporting Information), A549 cells (Figure S5B, Supporting Information), MDA-MB 231 cells (Figure S5C, Supporting Information), and MIA PaCa-2 cells (Figure S5D, Supporting Information), consistent with the downregulation of the selected biomarkers in these cancer cells. As measured by the mean fluorescence intensity (MFI) of cancer cells, the F-actin level was reduced 18%, 24%, 39%, and 29% in MCF-7 cells (Figure S5A, Supporting Information), A549 cells (Figure S5B, Supporting Information), MDA-MB 231 cells (Figure S5C, Supporting Information), and MIA PaCa-2 cells (Figure S5D, Supporting Information), respectively, after RP-ER treatment.

2.3. RP-ER Regulates the ECM Expression

To determine whether reduction of these biomarker expressions also occurred at the tissue level, the mice bearing HeLa tumors were treated with RP-ER. Significant reductions of mRNA levels of *EGFR*, *ITGAV*, and *ITGB3* were observed after treatment with RP-ER. In contrast, treatment with agents that

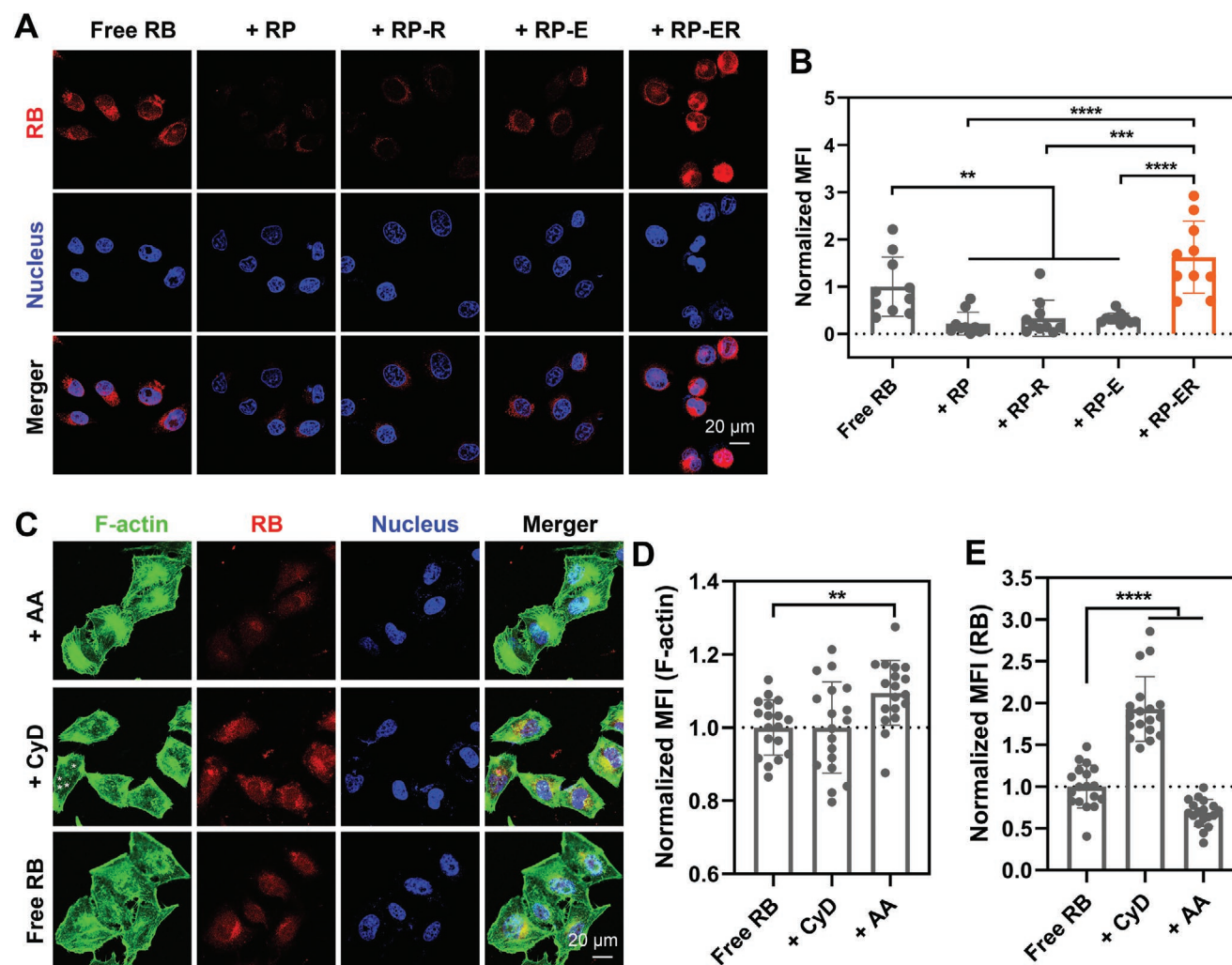


Figure 2. RP-ER enhances the cellular uptake of free RB in HeLa cells. A,B) The cellular uptake of free RB in HeLa cells in the presence of various RPs A) and their normalized MFI in cells (B) ($n = 10$). C–E) The free RB internalization by HeLa cells was improved with regulation of the F-actin content. HeLa cells with pretreatment of CyD or AA for 10 min were further incubated with same amount of free RB for another 4 h. The F-actin contents were visualized with FITC-labeled phalloidine C). The filaments of actin were truncated or generated by CyD or AA D). The cellular internalization of free RB E) was improved and reduced by CyD and AA, respectively ($n = 18$). Data are presented in mean \pm sd. P values were calculated using multiple t -tests. $**P < 0.01$, $***P < 0.001$, $****P < 0.0001$.

singularly targeted EGFR caused upregulation of the mRNA levels of *ITGAV* and *ITGB3* genes in HeLa tumors (Figure 3A), consistent with the finding that the activation of the integrin pathway is the compensation mechanism of anti-EGFR resistance.^[20] Furthermore, the expression levels of EGFR and $\alpha_v\beta_3$ in the tumor were lowered 49% and 67%, respectively, after RP-ER treatment, and displayed no significant differences when the mice were treated by RP, RP-R, and RP-E (Figure S6A,B, Supporting Information). Additionally, 60% reduction of F-actin and 90% reduction of collagen I synthesis were observed in the tumor that received RP-ER treatment compared to controls (Figure 3B,C). Moreover, the level of α -smooth muscle actin (α SMA), a biomarker of activated fibroblast cells, was significantly decreased by 86%, coupled with a 18% reduction of the expression of transforming growth factor β 1 (TGF β 1) (Figure 3B,C). Compared to the treatment with RP-E and RP-R that singularly targeted either EGFR or integrin, RP-ER

treatment reduced collagen I and activated fibroblast cells in tumors, suggesting a clear synergistic effect of the EGFR nanobody and RGD ligand on the RP-ER in downregulating EGFR, integrin, F-actin, collagen I, α SMA, and TGF β 1. The reductions of the expressions of F-actin, collagen I, and α SMA in tumor tissues were also observed in other types of xenograft tumors including MCF-7 tumors, A549 tumors, and MDA-MB 231 tumors (Figure S7, Supporting Information).

To further understand the mechanisms of RP-ER regulating the ECM in tumors, HeLa tumors treated with RP-ER were collected for proteomics analysis. Gene ontology (GO) and KEGG pathway analyses of the down-regulated-protein-related genes in RP-ER treated tumors revealed that the enriched annotation genes were associated with ECM and actin filament, suggesting that RP-ER treatment disrupts the ECM in TME and F-actin in cancer cells (Figure 3D). Histological staining of the harvested tumor tissues confirmed that the levels of collagen

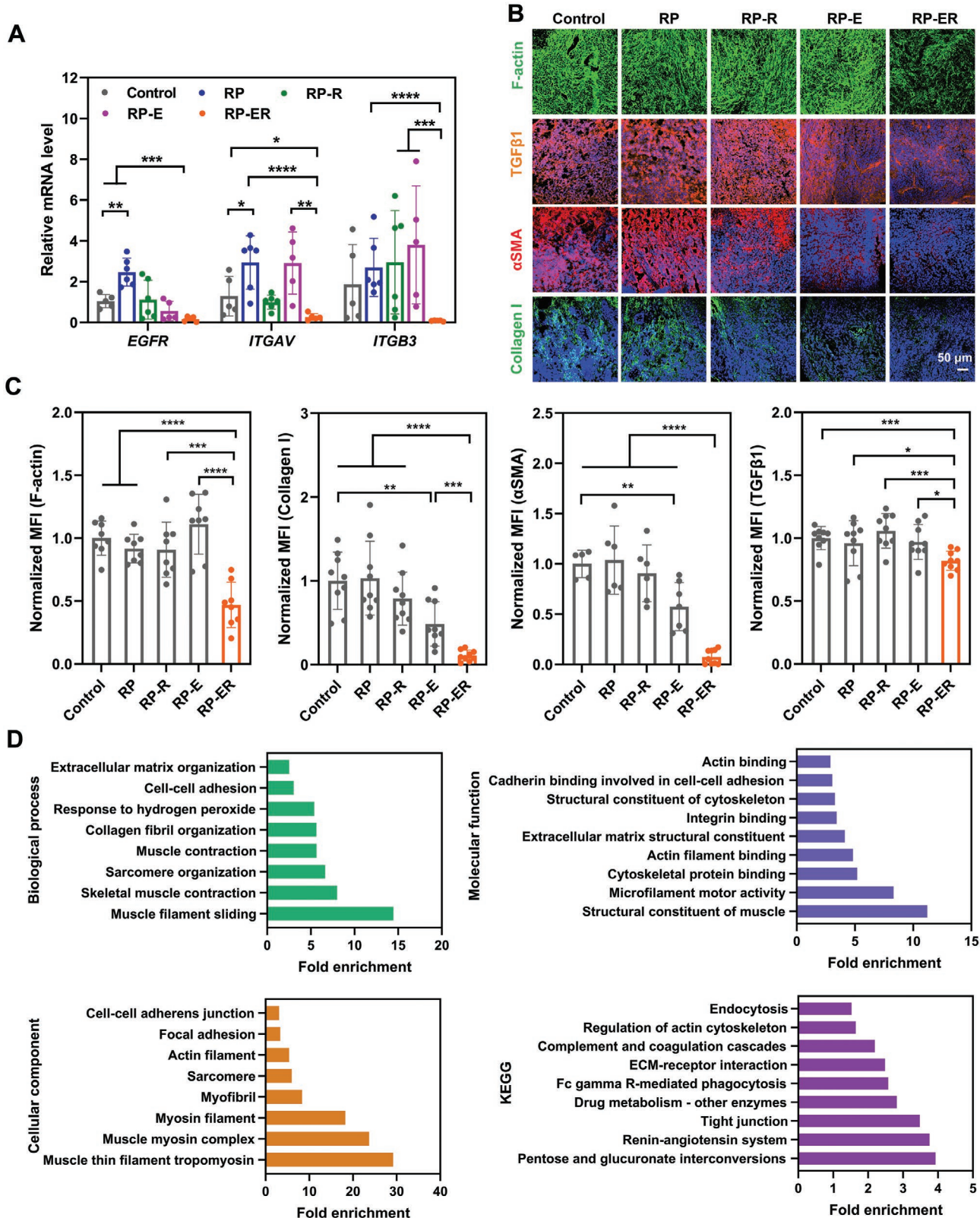


Figure 3. RP-ER regulates the ECM expression in the TME. A) The relative mRNA levels of *EGFR*, *ITGAV*, and *ITGB3* in HeLa tumors after treatment with various RPs ($n = 5-6$). Data are presented in mean \pm s.d. P values were calculated using multiple t -tests. $*P < 0.05$, $**P < 0.01$, $***P < 0.001$, $****P < 0.0001$. B,C) The expressions of F-actin, $TGF\beta 1$, αSMA , and collagen I in TME were measured by immunofluorescence B) and semiquantitatively analyzed based on the normalized MFI C) ($n = 5-9$). Data are presented in mean \pm s.d. P values were calculated using multiple t -tests. $*P < 0.05$, $***P < 0.001$, $****P < 0.0001$. D) Enriched annotation genes of the downregulated genes for RP-ER versus control based on GO and KEGG pathway analysis of mass spectrometry data.

were reduced after treatment with the dual-targeting RP-ER (Figure S6C,D, Supporting Information).

2.4. RP-ER Regulates Physical Properties of Tumors

Next, we examined the effect of different RPs on the interstitial fluid pressures (IFPs) and solid stresses of tumors, two characteristic mechanical properties of TME.^[44] In the HeLa tumors of the mice that received RP-ER treatment, IFP, and solid stress were found significantly decreased by 38% and 34%, respectively (Figure 4A,B). In sharp contrast, no changes in IFP and solid stress were observed in the tumors treated with RP and the single-targeting RP-E and RP-R. Notably, cetuximab used in the current cancer therapy can also lower the tumor IFP but has no significant effect on the tumor solid stress. More importantly, RP-ER treatment led to 53% reduction of the tumor stiffness measured by Young's modulus, while only 40% and 13% reductions of Young's modulus were observed in the tumors treated with RP-E and RP-R, respectively (Figure 4C). Similar changes in the physical properties of IFP, solid stress and Young's modulus were also found in MCF-7 (Figure S8A, Supporting Information), A549 (Figure S8B, Supporting Information), MDA-MB 231 (Figure S8C, Supporting Information), and MIA PaCa-2 (Figure S8D, Supporting Information) tumors after RP-ER treatment. Worth noting, the IFPs of MCF-7, A549, MDA-MB 231, and MIA PaCa-2 tumors were significantly reduced by 30%, 64%, 23%, and 41%, respectively (Figure S8, Supporting Information). In addition, solid stresses were decreased by 15%, 14%, 42%, and 26% for MCF-7, A549, MDA-MB 231, and MIA PaCa-2 tumors, respectively (Figure S8, Supporting Information). The RP-ER treatment reduced the Young's modulus of MCF-7, A549, MDA-MB 231, and MIA PaCa-2 tumors by 39%, 49%, 66%, and 63%, suggesting that RP-ER reduces the tumor stiffness (Figure S8, Supporting Information). Compared to RP-ER, RPDC-ER showed a similar effect on the reduction of the IFP and solid stress in MCF-7 tumors, suggesting that drug conjugation did not influence the tumor physical properties regulation capacity of RP-ER (Figure S8A, Supporting Information).

Taken together, these results indicate that the dual-targeting RP-ER simultaneously inhibited the expressions of both EGFR and $\alpha_v\beta_3$, leading to a synergistic disruption of tumor ECM by

altering FAK and F-actin signaling and reducing the contents of collagen I and activated fibroblast cells. Consequently, RP-ER remodels the physiological and physical properties of TME by relaxing the cytoskeleton tension of tumor cells and softening tumor ECM, as evidenced by the observed reduction of IFP, solid stress and Young's modulus of tumors.

2.5. RPDC-ER Enhances Transcellular Delivery and Intratumor Distribution of the Therapeutic Agents

In addition to disrupting the TME, dual-targeting RPDC can carry a therapeutic agent DOX, i.e., RPDC-ER, achieving increased intracellular and extracellular delivery compared to those integrin-targeting RPDC-R and EGFR-targeting RPDC-E or RPDC without any targeting moiety (Figure 5). RPDCs were detected and localized by the fluorescence of DOX and quantitatively analyzed by the MFIs. To evaluate the transcellular delivery capacity of RPDC-ER, we designed a sequential incubation experiment (Figure 5A). In the first round, cancer cells cultured on coverslip were incubated with different RPDCs. For the second round, the RPDCs treated cancer cells were transferred into a new chamber and incubated with cancer cells cultured on another coverslip. Then, the second coverslip was taken out, transferred into other chambers, and incubated with a third coverslip. After three rounds of coincubation with fresh medium and cancer cells, only the cells coincubated with RPDC-ER-treated cells still showed a strong fluorescent signal, suggesting dual-targeting RPDC-ER had the strongest transcellular transportation ability compared to the other RPDCs (Figure 5B,C).

To further evaluate the transcellular transportation efficacy, the DOX contents in each round were quantified by a fluorescence spectrophotometer. About 77.5% RPDC-ER in the cells in the first coverslip in round 1 was transported into round 2 including 48.3% transported into the cells and 29.2% transported into the medium in round 2 (Figure 5D). Only 22.5% RPDC-ER was left in the cells in the first coverslip, indicating the high transcellular transportation ability of RPDC-ER. In addition, 74.6% RPDC-ER in the cells in round 2 was transported into round 3, among which 28% RPDC-ER had been delivered into the cells in round 3 (Figure 5D). Further, an endocytosis pathways analysis indicated that all the RPDCs

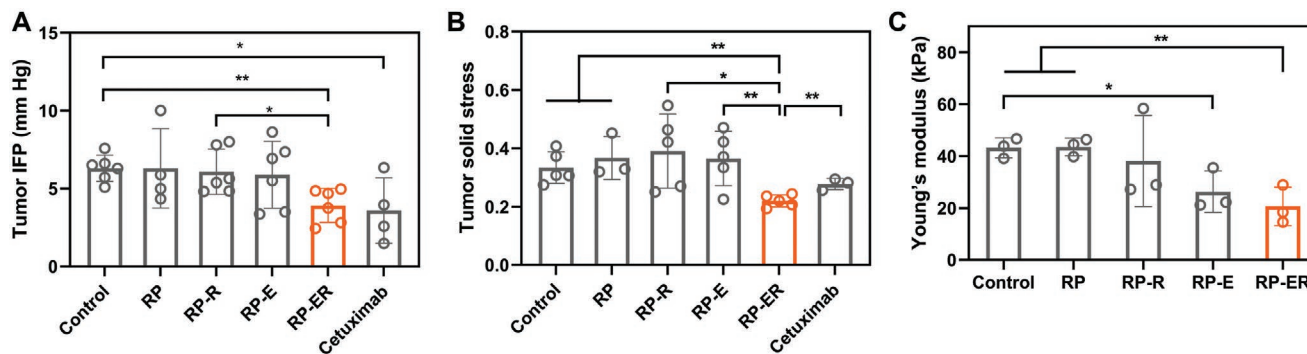


Figure 4. RP-ER changes the physical properties of HeLa tumors. A–C) The IFP A), solid stress B), and Young's modulus C) of HeLa tumors after treatment with various RPs ($n = 3–6$ tumors). Data are presented in mean \pm sd. P values were calculated using multiple t -tests. $*P < 0.05$, $**P < 0.01$.

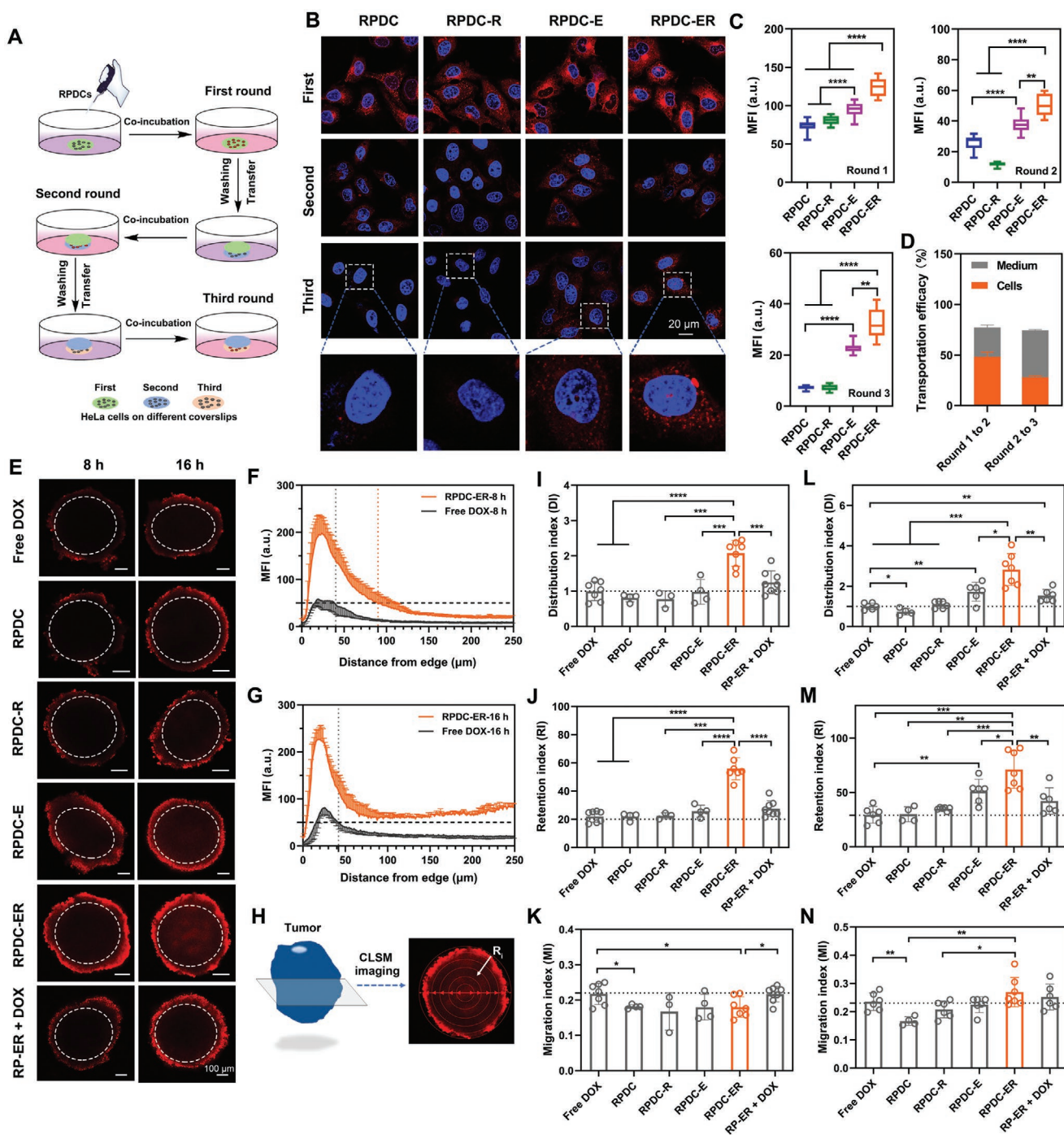


Figure 5. RPDC-ER enhances transcellular delivery and intratumor distribution of the therapeutic agents in 3D multicellular spheroids (MCs). A) The schematic diagram of experiments measuring transcellular transportation of different RPDCs in HeLa cells. B, C) The transcellular transportation of various RPDCs in HeLa cells shown in CLSM images B) and their MFIs analysis C) ($n = 10$). D) The transcellular transportation efficacy of RPDC-ER in HeLa cells evaluated by measuring the DOX contents in each round through a fluorescence spectrometer at an excitation/emission wavelength of 480 and 590 nm ($n = 4$). E) The CLSM images of HeLa MCs incubated with free DOX, RPDC, RPDC-R, RPDC-E, RPDC-ER, or RP-ER+free DOX after 8 and 16 h at 37 °C. F, G) The radial distribution of RPDC-ER and free DOX based on fluorescence intensity in HeLa MCs for 8 h F) and 16 h G) ($n = 3-7$). H) Schematically showing the regions for calculating RI, MI, and DI. The maximum focal plane of MCs in CLSM images for 8 h F) and 16 h G) was segmented into number of concentric circles with 50 μm radius interval. The minimum radius of circle was 50 μm . I-N) The DIs I, L), RIs J, M), and MIs K, N) of different agent after 8 h I-K) ($n = 3-8$) and 16 h L-N) ($n = 4-7$) incubation with HeLa MCs. Data are presented in mean \pm sd. P values were calculated using multiple t -tests. * $P < 0.05$, ** $P < 0.01$, *** $P < 0.001$, **** $P < 0.0001$.

can enter HeLa cells through caveolae-mediated endocytosis, clathrin-mediated endocytosis, and micropinocytosis (Figure S9, Supporting Information).

Multicellular spheroid (MC) is a vessel-free tumor model *in vitro* that can be used to mimic the cell–cell and cell–extracellular matrix interaction in the TME.^[45] When using HeLa MCs (diameter of 500 μm) to investigate the migration and distribution of RPDCs after 8 and 16 h incubations, EGFR and integrin dual-targeting RPDC-ER was found to migrate over a distance of 250 μm from the periphery of MCs after 16 h, much farther than 50 and 150 μm observed in the single-targeting RPDC-R and RPDC-E, respectively (Figure 5E–G; and Figure S10, Supporting Information). A time-dependent increase in fluorescence intensity and diffusion of RPDCs was observed in MCs. To quantitatively analyze the transport performance of RPDC-ER in MCs, we used three measurement parameters—migration index (MI), retention index (RI), and distribution index (DI)—to describe the spatial distribution, spheroid retention and a composition of migration and retention within tumor spheroids (Figure 5H–N). At both 8 and 16 h, RPDC-ER had the highest RI and DI among all the RPDCs. Coincubation with RP-ER and free DOX did not change the MI of free DOX, but improved the RI and DI of free DOX, indicating that RP-ER coincubation enhanced the distribution of DOX through enhanced retention over migration. All RPDCs showed an equivalent MI at 8 h (Figure 5K), however, the MI of RPDC-ER increased at 16 h, even though it was the largest molecular size (Figure 5N). Compared to free DOX, RPDC-ER exhibited the highest DI and RI as well as an equivalent MI, suggesting that the migration and retention of RPDCs were facilitated by the simultaneous blocking of EGFR and integrin by RPDC-ER (Figure 5H–N). No “binding site barrier” effect was observed for RPDC-ER.^[46]

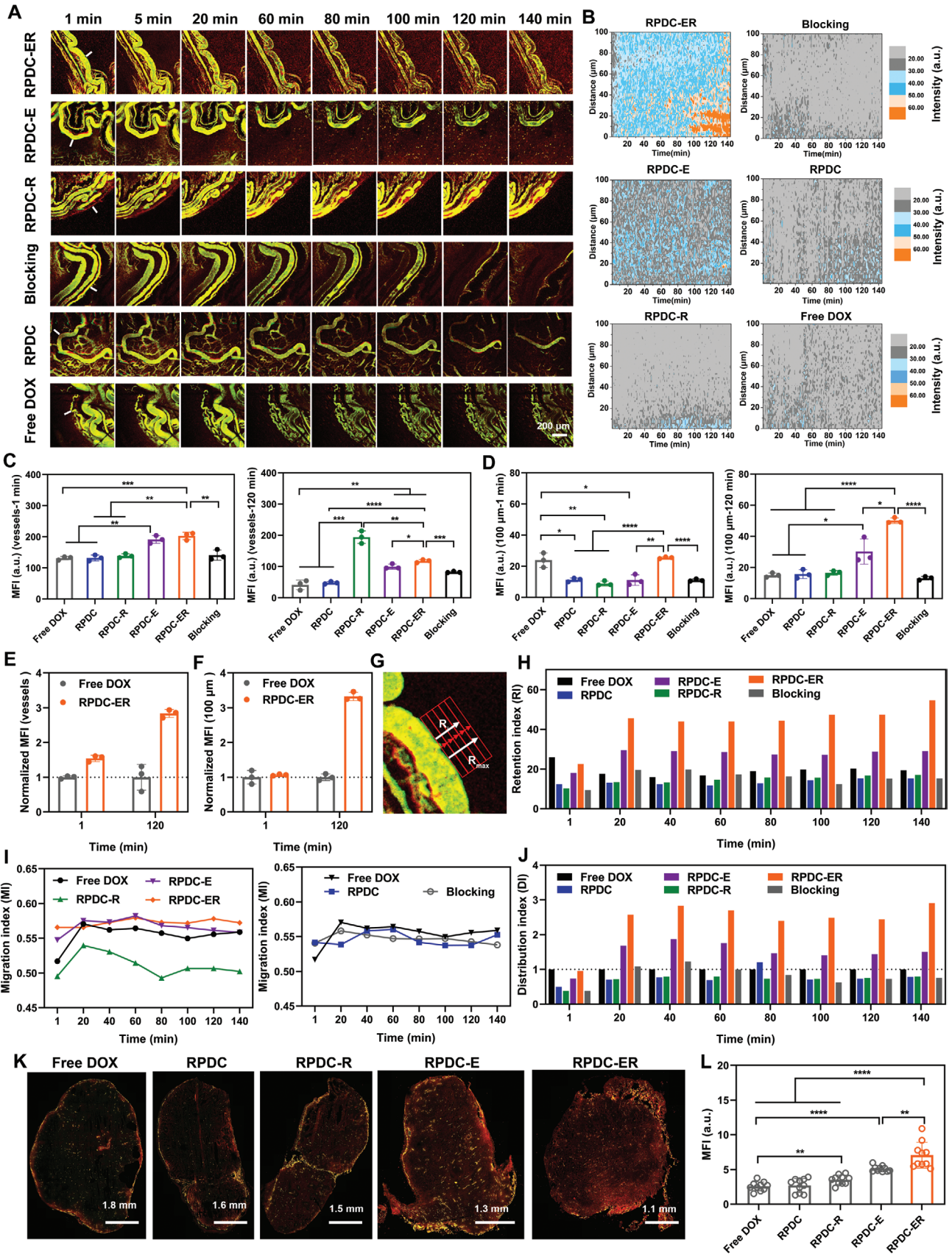
The real-time confocal laser scanning microscopy (CLSM) imaging of the HeLa xenograft tumors were collected from the tumor-bearing mice intravenously (i.v.) injected with different RPDCs. This revealed that the EGFR and integrin dual-targeting RPDC-ER showed the highest intratumor distribution, followed by EGFR-targeted RPDC-E (Figure 6A,B). RPDC-ER could reach regions 100 μm away from the tumor blood vessels 5 min after injection. Based on measurements of the fluorescence intensities of each RPDC within the blood vessels and tumor tissue 100 μm away from the vessel at different time points after injection, only RPDC-ER and RPDC-E exhibited continuous increase of extravascular fluorescence intensities in the tumor tissue over time with RPDC-ER exhibiting a more pronounced change (Figure 6C,D). The MFI inside vessels for RPDC-ER was higher than free DOX from 1 to 120 min after treatment (Figure 6E), indicating higher accumulation and retention of RPDC-ER. A 3-fold increase in extravascular MFI from RPDC-ER 120 min postinjection (Figure 6F) indicates that large RPDC-ER is more effectively diffused and retained in the tissues than small molecules after extravasating from the blood vessels, likely due to the disruption of ECM and softened tumor stiffness. In contrast, the integrin-targeting RPDC-R mostly accumulated in the vicinity of tumor vessels without diffusing farther away, likely due to the significant affinity of the integrin targeted RPDC-R to the integrin rich vasculature. When blocking EGFR targets with i.v. injection

of cetuximab in advance, RPDC-ER was largely found to accumulate in the regions close to the tumor blood vessels, similar to that observed in RPDC-R that only targets tumor integrin (Figure 6A–F).

To quantitatively analyze the transport performance of RPDC-ER in tumor, we also used MI, RI, and DI parameters mentioned in MCs model above to describe the spatial distribution, tissue retention, and a composition of migration and retention around the tumor blood vessels (Figure 6G–J). Different to MCs, we segmented the extravascular area into five of 200 \times 20 μm rectangular elements with the long side parallel to vessel and wide side located at different radial distances from the edge of the blood vessels (Figure 6G). The maximum distance away from the tumor blood vessel was 100 μm (5 \times 20 μm). The RI values changed with time for various RPDCs. The RI of RPDC-ER was at the same level as that of free DOX at 1 min postinjection, but this value became 2.6-fold over that of free DOX at 20 min and reached about three folds at 140 min (Figure 6H). Meanwhile, RPDC-ER showed the highest MI among all the RPDCs and free DOX (Figure 6I), suggesting that RPDC-ER has the best migration ability after vascular extravasation. Eventually, RPDC-ER exhibited the highest DIs at each time point postinjection except 1 min (Figure 6J), at 140 min postinjection, the DI value was threefold high than that of free DOX. This result indicates that RPDC-ER had the largest distribution in the extravascular areas in tumors. RPDC, RPDC-R, and RPDC-ER with EGFR blocking showed lower MIs and RIs than that of free DOX (Figure 6H,I). EGFR-targeted RPDC-E exhibited MIs at the same level as that of RPDC-ER but lower RIs than RPDC-ER, suggesting that RPDC-E has a similar migration ability to RPDC-ER but a less retention ability. RPDC, RPDC-R, and RPDC-ER with EGFR blocking displayed lower DIs than that of free DOX and only RPDC-ER and RPDC-E showed DIs larger than 1 (Figure 6J). Immunofluorescence staining of the sections from the whole tumors showed that RPDC-ER not only had the highest accumulation in the tumor but also the most homogeneous intratumor distribution compared to other RPDCs and free DOX (Figure 6K,L), also in agreement with the CLSM observation.

2.6. RPDC-ER Improves the Biodistribution of Therapeutic Agents and Antitumor Efficacy

The intratumor distributions of DOX in HeLa tumors delivered by RPDC, RPDC-E, RPDC-R, RPDC-ER at 1 h after i.v. injection of an equivalent dose of DOX at 5 mg kg⁻¹ were 2.0, 4.0, 3.5, and 14.5% ID g⁻¹, respectively, in comparison to 1.35% ID g⁻¹ for free DOX (Figure 7A; and Figure S11A, Supporting Information). Dual-targeting RPDC-ER showed the highest tumor accumulation with 11-fold over free DOX, sevenfold over RPDC, and fourfold over RPDC-R and RPDC-E, indicating the substantial improvement in tumor-specific delivery by dual-targeted RPDC-ER. In addition, RPDCs also significantly reduced the drug accumulation in normal tissues (Figure 7B; and Figure S11B–F, Supporting Information). At 1 h post-treatment, RPDC-ER reduced the drug contents in the heart, liver, lung about 3-fold, 1.8-fold, and 4.2-fold of free DOX, respectively (Figure 7B). Longitudinally, RPDC-ER reduced drug retention in the heart, liver, spleen, and lung from



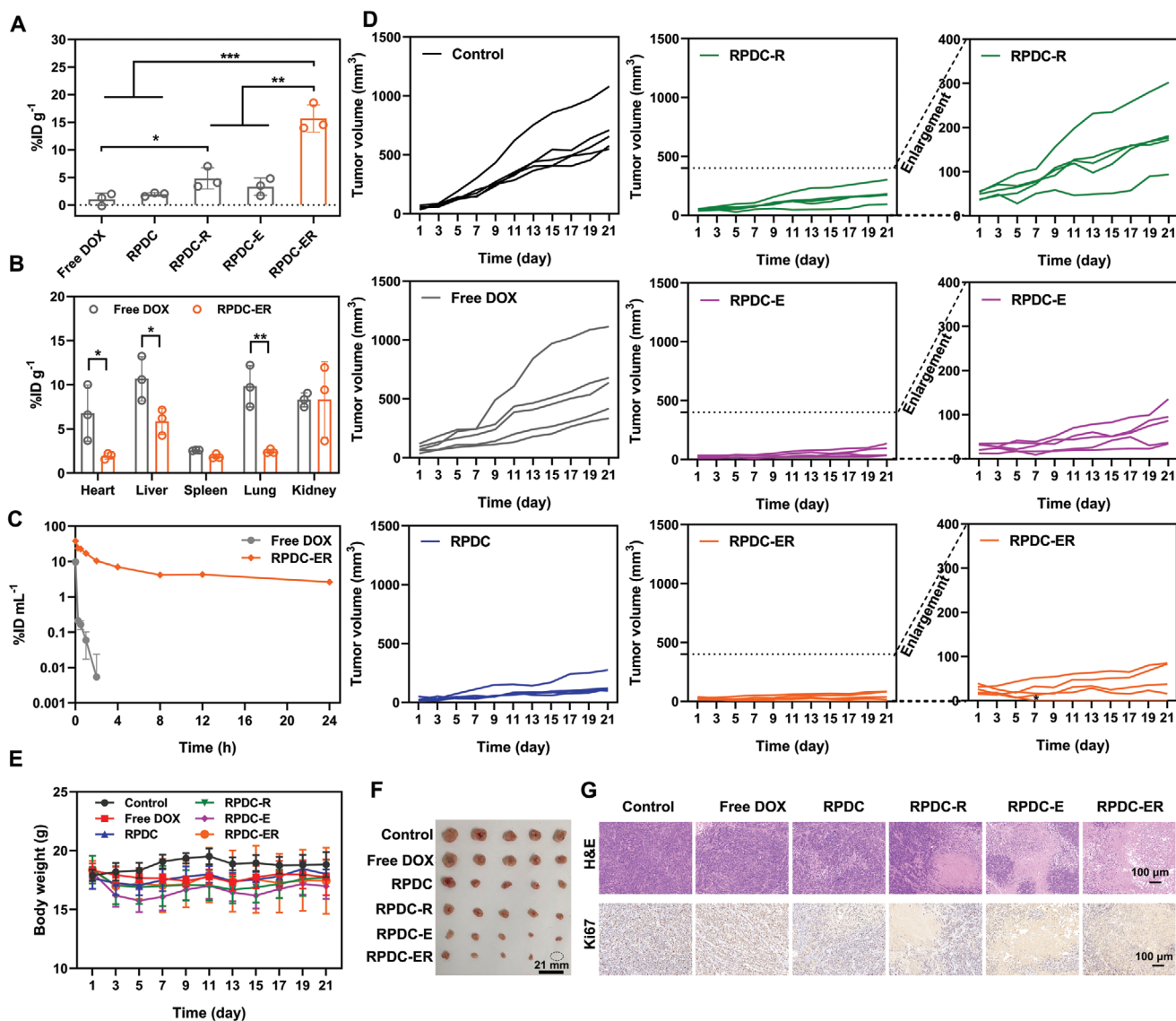


Figure 7. RPDC-ER improves the biodistribution of the therapeutic agents and antitumor efficacy. A) The DOX accumulation in HeLa tumors for different agents ($n = 3$). B) DOX accumulation in normal organs in the mice bearing HeLa tumors at 1 h postinjection of different treatments ($n = 3$). C) The pharmacokinetics of RPDC-ER and free DOX ($n = 3$). D) The growth curves of HeLa tumors after treatment with free DOX (5 mg kg^{-1}), RPDC (20 mg kg^{-1} , DOX eq.), RPDC-E (20 mg kg^{-1} , DOX eq.), RPDC-R (20 mg kg^{-1} , DOX eq.), RPDC-ER (20 mg kg^{-1} , DOX eq.) ($n = 5$). E) The body weights of mice bearing HeLa tumors treated with different agents ($n = 5$). F) Images of the tumors collected from mice with different treatments at day 21. G) Representative images of the tumor sections examined by H&E or Ki67 staining at day 21 postinjection of different treatments. Data are presented in mean \pm sd. P values were calculated using multiple t -tests. * $P < 0.05$, ** $P < 0.01$, *** $P < 0.001$.

1 to 24 h after drug injection (Figure S11B–E, Supporting Information) and metabolized out of body through the kidneys similar to free DOX (Figure S11F, Supporting Information).

The pharmacokinetic behaviors of free DOX and RPDCs were evaluated in healthy ICR mice (Figure 7C; and Figure S11G–I, Supporting Information). For free DOX, the

Figure 6. RPDC-ER enhances intratumor distribution of the therapeutic agents in xenograft tumors. A) Vascular extravasation and diffusion of RPDC-ER, RPDC-E, RPDC-R, cetuximab-pretreated RPDC-ER (Blocking), RPDC, and free DOX at different time points after i.v. injection into HeLa tumor-bearing mice. B) Distribution of RPDCs and free DOX away from the blood vessels at different time points and distances. A region marked with the rectangular frame in A) was selected for the analysis. C,D) The MFIs of three regions of interest inside tumor vessels C) and 100 μm away from vessels D) for RPDC, RPDC-E, RPDC-R, RPDC-ER, cetuximab-pretreated RPDC-ER (Blocking) and free DOX at 1 and 120 min postinjection ($n = 3$). E,F) The normalized MFIs measured inside vessels and at 100 μm away from the tumor vessel for RPDC-ER and free DOX at 1 E) and 120 F) min postinjection ($n = 3$). G) Schematically showing the regions for calculating RI, MI, and DI. The extravascular area was segmented into five of $200 \times 200 \mu\text{m}^2$ rectangle elements located at different radial distance from the edge of the blood vessels. The maximum distance was designed as 100 μm ($5 \times 20 \mu\text{m}$). H–J) The calculated RIs H), MIs I), and DIs J) of different agents at different time points after i.v. injection into HeLa tumor-bearing mice. K) Intratumor distribution of RPDCs in the whole HeLa tumors after treatment for 16 h. L) The MFIs measured in the areas ($200 \times 200 \mu\text{m}^2$) outside vessels (100 μm away from vessels) ($n = 3$). Data are presented in mean \pm s.d. P values were calculated using multiple t -tests. * $P < 0.05$, ** $P < 0.01$, *** $P < 0.001$, **** $P < 0.0001$.

DOX concentration in blood decreased rapidly. However, the DOX concentration in blood could still be detected at 24 h postinjection for RPDC-ER. RPDC-ER prolonged the circulation time of free DOX from 0.5 to 22 h (noncompartmental model) (Figure 7C).^[47] Given that the conjugates sufficiently lowered the drug accumulation in healthy organs, we first investigated the maximum tolerated dose (MTD) of RPDCs on healthy ICR mice before evaluating the anticancer effect. Compared to free DOX, the MTD of conjugates increased 4 fold (Figure S12A–E, Supporting Information). No statistically significant change in serum biochemical indexes and injury to major organs was observed at the MTD (Figure S12F,G, Supporting Information).

Overall, the improved tumor-targeted delivery and intratumor distribution by the dually targeting EGFR and integrin $\alpha_v\beta_3$ with RPDC-ER led to the higher antitumor efficiency in treating HeLa tumors than the singular-targeting RPDCs of similar structure (i.e., RPDC-E and RPDC-R) (Figure 7D; and Figure S13, Supporting Information) with negligible side effects (Figure 7E). Tumors in the control group and free DOX group grew rapidly. Compared to the control group and free DOX group, the inhibition of tumors in RPDC group and RPDC-R group was limited. In contrast, RPDC-E showed a better antitumor effect. Interestingly, dual-targeting RPDC-ER exhibited the best antitumor effect among the RPDCs and one tumor was even eradicated at Day 7 with only one injection. The average tumor volumes measured at 21 days after the treatment with RPDC-ER, RPDC-E, RPDC-R, RPDC, free DOX and PBS, were 1.6, 2.8, 3.9, 6.6, 8.2, and 16 times, respectively, compared to those on day 1. The tumors treated with RPDC-ER were the smallest (Figure 7F) with the largest necrosis area and lowest proliferation (Figure 7G). These data suggest that RPDC-ER has significantly better efficacy in impeding tumor growth and reducing side effects, a result of softened tumor ECM and disrupted TME based on mRMM–ECM strategy.

3. Discussion and Conclusion

ECM is a key regulator of tissue organization and homeostasis, playing important roles in the regulation of cell behaviors and cell transport in tissues.^[2,48] The molecules of ECM interact with each other to create a dense meshwork that dynamically interacts with cell surface receptors on residing cells. Previous studies have revealed some mechanistic insights into the effects of ECM on cancer cell actions and functions in TME, providing potential strategies to target ECM in treating cancers. However, these investigations were mostly focused on how ECM stiffness regulates tumor cell proliferation, invasion, and metastatic dissemination as well as stem cell activation and differentiation.^[11,14,16] Different from these studies, we showed that tumor cells also can affect and modulate ECM, and eventually TME. By simultaneously blocking cell surface receptors on resident cancer cells, cell–matrix interactions could be disrupted. Our results suggest an intriguing mechanism that simultaneously inhibit tumor cell receptor EGFR and integrin $\alpha_v\beta_3$ and leads to a network change of cancer cell signaling molecules including FAK and F-actin, and subsequent reduction of tumor ECM components, such as collagen I, TGF β 1, and α SMA. As a result, TME was profoundly disrupted. The decreased IFP, solid

stress and stiffness of tumors due to disruption of TME allows for extended intratumor distribution, increased cellular uptake processes and transcellular transportation of RPDCs in tumors.

As the key coupling points between ECM and cancer cells, integrins largely influence intracellular and extracellular biochemical and mechanical signals.^[19,49,50] Inhibiting tumor integrin and EGFR by dual-targeting RPDCs down-regulates the levels of FAK and F-actin, lessening the cytoskeletal tension and allowing for increased internalization and transcellular transportation of drug molecules in cancer cells. Blocking integrin and EGFR not only lowered the contents of collagen I, TGF β 1, and α SMA in ECM, but also decreased adhesions between collagens and tumor cells. As a result of reducing the tension of the collagens and collagen network, drug molecules, or other therapeutic agents can readily diffuse within the tumor tissue matrix. Thus, the therapeutic response toward cancers can be significantly improved.

ECM is a physical and biological obstacle for drug penetration into deep tumor tissue. Abundant ECM, including 80% collagens leads to a compact TME with an elevated IFP and solid stresses, impeding drug delivery into the tumor mass.^[51] Disrupting the ECM to remove the stromal barriers in TME is a feasible way to improve the drug reaching the tumor. However, extensive studies were focused on the ECM degradation directly, including enzymatic degradation of hyaluronan,^[52] decreasing fibroblast activation,^[53] inhibiting ECM cross-linking,^[7] and degradation of collagen with collagenase.^[54] How the receptors of cancer cells affect the ECM, especially how blocking receptors disrupt the ECM, is poorly understood. Here, we show that two cancer cell receptors, EGFR and integrin, play a key role on the ECM expressions in the TME. By simultaneously blocking EGFR and integrin, RPDC-ER was able to disrupt ECM in the TME, regulate physical properties including reduction of IFP and solid stress, and soften tumors, enhancing drug migration, retention and distribution in tumor tissues. With this mRMM–ECM approach, we showed that RPDC-ER could rapidly extravasate from blood vessels into tumor mass and deliver drugs far away from blood vessels and enhance transcellular delivery. The mRMM–ECM approach proposed in this study would be helpful for furthering understanding of the synergistic effects between these two receptors and for furthering applications in regulating cancer cells through receptors to enhance drug delivery.

In summary, this new approach of mRMM–ECM highlighted by simultaneous targeting of EGFR and tumor integrin can regulate TME through the disruption of ECM to improve the delivery of therapeutic agents and even directly increase the efficacy of existing cancer treatments that are limited by TME. The simultaneous targeting is achieved by installing an EGFR nanobody and integrin ligand together on a rationally designed RP and RPDC platform. The mRMM–ECM approach and the RPDC platform presented in this study may be applied in the future design of therapeutic antibodies and antibody–drug conjugates for targeting TME to increase intratumor delivery and distribution and overcome the “binding site barrier” that limits the delivery of antibodies and antibody–drug conjugates in to tumors.

Supporting Information

Supporting Information is available from the Wiley Online Library or from the author.

Acknowledgements

This study was supported by the National Key R&D Program of China (Nos. 2017YFA0701301 and 2017YFA0205400), the Natural Science Foundation of China (Nos. 92163214, 51690153, 21720102005, and 51803089), and the Natural Science Foundation of Jiangsu Province (No. BK20202002). All animal experiments were performed in compliance with guidelines set by the Animal Ethical and Welfare Committee at Nanjing University (Nanjing, China) (ID: 2003100).

Conflict of Interest

The authors declare no conflict of interest.

Data Availability Statement

The data that support the findings of this study are available from the corresponding author upon reasonable request.

Keywords

drug delivery, drug distribution, tumor environment, tumor extracellular matrix

Received: November 18, 2021

Revised: December 25, 2021

Published online: January 31, 2022

- [1] O. Chaudhuri, J. Cooper-White, P. A. Janmey, D. J. Mooney, V. B. Shenoy, *Nature* **2020**, *584*, 535.
- [2] C. Bonnans, J. Chou, Z. Werb, *Nat. Rev. Mol. Cell Biol.* **2014**, *15*, 786.
- [3] B. Trappmann, J. E. Gautrot, J. T. Connelly, D. G. T. Strange, Y. Li, M. L. Oyen, M. A. Cohen Stuart, H. Boehm, B. Li, V. Vogel, J. P. Spatz, F. M. Watt, W. T. S. Huck, *Nat. Mater.* **2012**, *11*, 642.
- [4] J. Winkler, A. Abisoye-Ogunniyan, K. J. Metcalf, Z. Werb, *Nat. Commun.* **2020**, *11*, 5120.
- [5] O. Chaudhuri, S. T. Koshy, C. Branco da Cunha, J.-W. Shin, C. S. Verbeke, K. H. Allison, D. J. Mooney, *Nat. Mater.* **2014**, *13*, 970.
- [6] A. Elosegui-Artola, R. Oria, Y. Chen, A. Kosmalska, C. Pérez-González, N. Castro, C. Zhu, X. Trepast, P. Roca-Cusachs, *Nat. Cell Biol.* **2016**, *18*, 540.
- [7] O. Saatci, A. Kaymak, U. Raza, P. G. Ersan, O. Akbulut, C. E. Banister, V. Sikirzhyski, U. M. Tokat, G. Aykut, S. A. Ansari, H. T. Dogan, M. Dogan, P. Jandaghi, A. Isik, F. Gundogdu, K. Kosemehmetoglu, O. Dizdar, S. Aksoy, A. Akyol, A. Uner, P. J. Buckhaults, Y. Riazalhosseini, O. Sahin, *Nat. Commun.* **2020**, *11*, 2416.
- [8] K. R. Levental, H. Yu, L. Kass, J. N. Lakins, M. Egeblad, J. T. Emler, S. F. T. Fong, K. Csizsar, A. Giaccia, W. Weninger, M. Yamauchi, D. L. Gasser, V. M. Weaver, *Cell* **2009**, *139*, 891.
- [9] M. J. Paszek, N. Zahir, K. R. Johnson, J. N. Lakins, G. I. Rozenberg, A. Gefen, C. A. Reinhart-King, S. S. Margulies, M. Dembo, D. Boettiger, D. A. Hammer, V. M. Weaver, *Cancer Cell* **2005**, *8*, 241.
- [10] J.-W. Shin, D. J. Mooney, *Proc. Natl. Acad. Sci. USA* **2016**, *113*, 12126.
- [11] S. C. Wei, L. Fattet, J. H. Tsai, Y. Guo, V. H. Pai, H. E. Majeski, A. C. Chen, R. L. Sah, S. S. Taylor, A. J. Engler, J. Yang, *Nat. Cell Biol.* **2015**, *17*, 678.
- [12] M. Saxena, S. Liu, B. Yang, C. Hajal, R. Changede, J. Hu, H. Wolfenson, J. Hone, M. P. Sheetz, *Nat. Mater.* **2017**, *16*, 775.
- [13] Y. Shen, X. Wang, J. Lu, M. Salfenmoser, N. M. Wirsik, N. Schleussner, A. Irmle, A. Freire Valls, P. Radhakrishnan, J. Liang, G. Wang, T. Muley, M. Schneider, C. Ruiz de Almodovar, A. Diz-Muñoz, T. Schmidt, *Cancer Cell* **2020**, *37*, 800.
- [14] R. S. Stowers, A. Shcherbina, J. Israeli, J. J. Gruber, J. Chang, S. Nam, A. Rabiee, M. N. Teruel, M. P. Snyder, A. Kundaje, O. Chaudhuri, *Nat. Biomed. Eng.* **2019**, *3*, 1009.
- [15] T. Panciera, A. Citron, D. Di Biagio, G. Battilana, A. Gandin, S. Giullitti, M. Forcato, S. Bicciato, V. Panzetta, S. Fusco, L. Azzolin, A. Tataro, A. P. Dei Tos, M. Fassan, V. Vindigni, F. Bassetto, A. Rosato, G. Brusatin, M. Cordenonsi, S. Piccolo, *Nat. Mater.* **2020**, *19*, 797.
- [16] J. Schrader, T. T. Gordon-Walker, R. L. Aucott, M. van Deemter, A. Quaas, S. Walsh, D. Bente, S. J. Forbes, R. G. Wells, J. P. Iredale, *Hepatology* **2011**, *53*, 1192.
- [17] O. Chaudhuri, L. Gu, D. Klumpers, M. Darnell, S. A. Bencherif, J. C. Weaver, N. Huebsch, H.-p. Lee, E. Lippens, G. N. Duda, D. J. Mooney, *Nat. Mater.* **2016**, *15*, 326.
- [18] J. S. Desgrosellier, L. A. Barnes, D. J. Shields, M. Huang, S. K. Lau, N. Prévost, D. Tarin, S. J. Shattil, D. A. Cheresh, *Nat. Med.* **2009**, *15*, 1163.
- [19] L. Seguin, J. S. Desgrosellier, S. M. Weis, D. A. Cheresh, *Trends Cell Biol.* **2015**, *25*, 234.
- [20] L. Seguin, S. Kato, A. Franovic, M. F. Camargo, J. Lesperance, K. C. Elliott, M. Yebra, A. Mielgo, A. M. Lowy, H. Husain, T. Cascone, L. Diao, J. Wang, I. I. Wistuba, J. V. Heymach, S. M. Lippman, J. S. Desgrosellier, S. Anand, S. M. Weis, D. A. Cheresh, *Nat. Cell Biol.* **2014**, *16*, 457.
- [21] C. Zeltz, D. Gullberg, *J. Cell Sci.* **2016**, *129*, 1284.
- [22] S. Affo, L.-X. Yu, R. F. Schwabe, *Annu. Rev. Pathol.: Mech. Dis.* **2017**, *12*, 153.
- [23] A. D. Theocharis, S. S. Skandalis, C. Gialeli, N. K. Karamanos, *Adv. Drug Delivery Rev.* **2016**, *97*, 4.
- [24] R. I. Nicholson, J. M. W. Gee, M. E. Harper, *Eur. J. Cancer* **2001**, *37*, 9.
- [25] T. Rao, V. P.-Y. Ma, A. Blanchard, T. Urner, S. Grandhi, K. Salaita, A. Mattheyses, *J. Cell Sci.* **2020**, *133*, jcs.238840.
- [26] B. Diop-Frimpong, V. P. Chauhan, S. Krane, Y. Boucher, R. K. Jain, *Proc. Natl. Acad. Sci. USA* **2011**, *108*, 2909.
- [27] H. Salmon, K. Franciszkiwicz, D. Damotte, M.-C. Dieu-Nosjean, P. Validire, A. Trautmann, F. Mami-Chouaib, E. Donnadieu, *J. Clin. Invest.* **2012**, *122*, 899.
- [28] I. Eke, K. Zscheppang, E. Dickreuter, L. Hickmann, E. Mazzeo, K. Unger, M. Krause, N. Cordes, *J. Natl. Cancer I.* **2015**, *107*, 1.
- [29] G. Covarrubias, F. He, S. Raghunathan, O. Turan, P. M. Peiris, W. P. Schiemann, E. Karathanasis, *PLoS One* **2019**, *14*, e0220474.
- [30] J. Vansteenkiste, F. Barlesi, C. F. Waller, J. Bannoun, C. Gridelli, E. Goekkurt, D. Verhoeven, A. Szczesna, M. Feurer, J. Milanowski, P. Germonpre, H. Lena, D. Atanackovic, M. Krzakowski, C. Hicking, J. Straub, M. Picard, W. Schuette, K. O'Byrne, *Ann. Oncol.* **2015**, *26*, 1734.
- [31] A. Bell, Z. J. Wang, M. Arbabi-Ghahroudi, T. A. Chang, Y. Durocher, U. Trojahn, J. Baardsnes, M. L. Jaramillo, S. Li, T. N. Baral, M. O'Connor-McCourt, R. MacKenzie, J. Zhang, *Cancer Lett.* **2010**, *289*, 81.
- [32] K. N. Sugahara, T. Teesalu, P. P. Karmali, V. R. Kotamraju, L. Agemy, D. R. Greenwald, E. Ruoslahti, *Science* **2010**, *328*, 1031.
- [33] J. A. MacKay, M. Chen, J. R. McDaniel, W. Liu, A. J. Simnick, A. Chilkoti, *Nat. Mater.* **2009**, *8*, 993.
- [34] S. Steeland, R. E. Vandenbroucke, C. Libert, *Drug Discovery Today* **2016**, *21*, 1076.
- [35] G. Bao, M. Tang, J. Zhao, X. Zhu, *EJNMMI Res.* **2021**, *11*, 6.
- [36] C. M. Bishop, W. F. Walkenhorst, W. C. Wimley, *J. Mol. Biol.* **2001**, *309*, 975.
- [37] H. Nuhn, H.-A. Klok, *Biomacromolecules* **2008**, *9*, 2755.
- [38] X. Zheng, H. Mao, D. Huo, W. Wu, B. Liu, X. Jiang, *Nat. Biomed. Eng.* **2017**, *1*, 0057.

- [39] P. Shi, Z. Liu, K. Dong, E. Ju, J. Ren, Y. Du, Z. Li, X. Qu, *Adv. Mater.* **2014**, *26*, 6635.
- [40] D. J. Sieg, C. R. Hauck, D. Ilic, C. K. Klingbeil, E. Schaefer, C. H. Damsky, D. D. Schlaepfer, *Nat. Cell Biol.* **2000**, *2*, 249.
- [41] L. He, E. J. Sayers, P. Watson, A. T. Jones, *Sci. Rep.* **2018**, *8*, 7318.
- [42] Y. Zhao, K. Pal, Y. Tu, X. Wang, *J. Am. Chem. Soc.* **2020**, *142*, 6930.
- [43] M. P. Peppelenbosch, L. G. J. Tertoolen, W. J. Hage, S. W. de Laat, *Cell* **1993**, *74*, 565.
- [44] H. T. Nia, H. Liu, G. Seano, M. Datta, D. Jones, N. Rahbari, J. Incio, V. P. Chauhan, K. Jung, J. D. Martin, V. Askoxylakis, T. P. Padera, D. Fukumura, Y. Boucher, F. J. Hornicek, A. J. Grodzinsky, J. W. Baish, L. L. Munn, R. K. Jain, *Nat. Biomed. Eng.* **2016**, *1*, 0004.
- [45] G. Mehta, A. Y. Hsiao, M. Ingram, G. D. Luker, S. Takayama, *J. Controlled Release* **2012**, *164*, 192.
- [46] M. Juweid, R. Neumann, C. Paik, M. J. Perez-Bacete, J. Sato, W. van Osdol, J. N. Weinstein, *Cancer Res.* **1992**, *52*, 5144.
- [47] Y. Zhang, M. Huo, J. Zhou, S. Xie, *Comput. Methods Programs Biomed.* **2010**, *99*, 306.
- [48] O. Chaudhuri, L. Gu, M. Darnell, D. Klumpers, S. A. Bencherif, J. C. Weaver, N. Huebsch, D. J. Mooney, *Nat. Commun.* **2015**, *6*, 6365.
- [49] J. D. Humphries, M. R. Chastney, J. A. Askari, M. J. Humphries, *Curr. Opin. Cell Biol.* **2019**, *56*, 14.
- [50] J. Z. Kechagia, J. Ivaska, P. Roca-Cusachs, *Nat. Rev. Mol. Cell Biol.* **2019**, *20*, 457.
- [51] C.-H. Heldin, K. Rubin, K. Pietras, A. Östman, *Nat. Rev. Cancer* **2004**, *4*, 806.
- [52] P. P. Provenzano, C. Cuevas, A. E. Chang, V. K. Goel, D. D. Von Hoff, S. R. Hingorani, *Cancer Cell* **2012**, *21*, 418.
- [53] K. Y. Elahi-Gedwillo, M. Carlson, J. Zettervall, P. P. Provenzano, *Cancer Res.* **2019**, *79*, 372.
- [54] A. Zinger, L. Koren, O. Adir, M. Poley, M. Alyan, Z. Yaari, N. Noor, N. Krinsky, A. Simon, H. Gibori, M. Krayem, Y. Mumblat, S. Kasten, S. Ofir, E. Fridman, N. Milman, M. M. Lübtow, L. Liba, J. Shklover, J. Shainsky-Roitman, Y. Binenbaum, D. Hershkovitz, Z. Gil, T. Dvir, R. Luxenhofer, R. Satchi-Fainaro, A. Schroeder, *ACS Nano* **2019**, *13*, 11008.